Vibrational Mode Structure and Symmetry in Proteins and Analogues Containing Fe_4S_4 Clusters: Resonance Raman Evidence for Different Degrees of Distortion in HiPIP and Ferredoxin

Roman S. Czernuszewicz, Kathleen A. Macor, Michael K. Johnson,† Andrew Gewirth, and Thomas G. Spiro*

Contribution from the Department of Chemistry, Princeton University, Princeton, New Jersey 08544. *Received March 20, 1987*

Abstract: Resonance Raman (RR) spectra are reported for $(Et_4N)_2[Fe_4S_4(SCH_2Ph)_4]$ in polycrystalline samples and in dimethylacetamide solution. RR spectra are also reported for high-potential iron protein (HiPIP) from *Chromatium vinosum* and for ferredoxin (Fd) from *Clostridium pasteurianum*, the latter being reconstituted with ^{34}S and ^{54}Fe for isotope shift measurements. The Fe–S stretching modes of polycrystalline $(Et_4N)_2[Fe_4S_4(SCH_2Ph)_4]$ have been completely assigned via the ^{34}S spectral shifts and the descent in symmetry from T_d to D_{2d}. These assignments are supported by the normal mode calculation, using a Urey–Bradley force field, which accurately reproduces the frequencies and isotope shifts. In solution, the RR spectrum of $(Et_4N)_2[Fe_4S_4(SCH_2Ph)_4]$ shows a tetrahedral pattern. The strongest evidence against significant symmetry lowering is the lack of activation of the cluster E mode, which is associated with the D_{2d} distortion, and is seen clearly in the crystal spectrum. The RR spectrum of oxidized Fd is very similar to that of crystalline $(Et_4N)_2[Fe_4S_4(SCH_2Ph)_4]$, and it shows clear evidence for a D_{2d} distortion, consistent with the X-ray crystal structure of the *Peptococcus aerogenes* Fd. On the other hand, the RR spectrum of HiPIP is nearly the same as that of $(Et_4N)_2[Fe_4S_4(SCH_2Ph)_4]$ in solution, but some evidence for the D_{2d} distortion is indicated by weak activation of the E cluster mode. The functional significance, if any, of the observed Fd versus HiPIP structural difference is discussed. Excitation profiles for terminal and bridging Fe–S modes of $(Et_4N)_2[Fe_4S_4(SCH_2Ph)_4]$ show maxima at ~450 nm, in a rising portion of the electronic absorption band and a decline at the absorption maximum, ~420 nm. This fall-off is suggested to result from interference effects among the charge-transfer transitions contained in the absorption band.

Proteins containing iron and sulfide and/or cysteine thiolate are ubiquitous biological electron transport agents and also function in hydrogen evolution and nitrogen reduction.[1] They occur in several structural variants, among which one of the most common is the Fe_4S_4 "cube", containing interpenetrating Fe_4 and S_4 tetrahedra, the Fe corners of which are bound to cysteinate sulfur atoms. This structure has been established by X-ray crystallography in three proteins:[2] ferredoxin (Fd) from *Peptococcus aerogenes* (*Pa*)[3] with two such clusters and "high-potential" iron protein (HiPIP) from *Chromatium vinosum* (*Cv*)[4] and *Azotobacter vinelandii* (*Av*) Fd I,[5] each with one such cluster.

The syntheses by Holm and co-workers[6] of Fe_4S_4 cubes with thiolate or halide replacing the protein cysteinate ligands has established that, under ordinary conditions, the stable oxidation level is $[Fe_4S_4]^{2+}$, in which the average oxidation state of the iron is $Fe^{2.5+}$, if the sulfur is counted as S^{2-}. The total electron count is even, and the clusters are observed to be diamagnetic. Alternative electronic structures have been described.[7] In proteins an electron can be removed or added at high or low potentials, respectively.[6-8] Apparently HiPIP ($E_{1/2}$ = +350 mV) operates at the $[Fe_4S_4]^{3+}/[Fe_4S_4]^{2+}$ oxidation levels, since it is paramagnetic in the oxidized but diamagnetic in the reduced form, while Fd ($E_{1/2}$ = −350 to −450 mV) operates at the $[Fe_4S_4]^{2+}/[Fe_4S_4]^{+}$ levels, since it is diamagnetic in the oxidized but paramagnetic in the reduced form. Synthetic analogues, $Fe_4S_4(SR)_4^{n-}$, have been isolated for n = 2 and 3.[6] Clusters with n = 1 have been detected electrochemically[9] and have recently been isolated and characterized.[10] For model complexes the n = 2−/3− process occurs at half-wave potentials, $E_{1/2}$, of 1 V or greater.[9b,10] Evidently the protein matrix stabilizes $[Fe_4S_4]^{3+}$ in HiPIP and $[Fe_4S_4]^{+}$ in Fd. Different numbers of H bonds, as deduced from X-ray structures, have been suggested to be responsible for the differential stabilization.[8,11]

The question has also arisen whether the proteins' architecture might favor one or the other of the structural distortions observed in X-ray crystal structures of complexes containing $[Fe_4S_4]^{2+}$ and $[Fe_4S_4]^{+}$ core oxidation levels.[6,12] The former has been examined for SCH_2Ph^-,[13] SPh^-,[14] $SCH_2CH_2OH^-$,[15] $SCH_2CH_2O_2^{2-}$,[16] S-*t*-

* Author to whom correspondence should be addressed.
† Present address: Department of Chemistry, University of Georgia, Athens, Georgia 30602.

(1) *Iron-Sulfur Proteins*; Lovenberg, W., Ed.; Academic: New York, 1973–1977; Vol. 1–3.
(2) Stout, C. D. In *Metal Ions in Biology*, Spiro, T. G., Ed.; Wiley-Interscience: New York, 1982; Vol. 4, Chapter 3.
(3) Adman, E. t.; Sieker, L. C.; Jensen, L. H. *J. Biol. Chem.* **1973**, *248*, 3987–3996; **1976**, *251*, 3801–3806.
(4) (c) Carter, C. W., Jr.; Kraut, J.; Freer, S. T.; Xuong, N. H.; Alden, R. A.; Bartsch, R. G. *J. Biol. Chem.* **1974**, *249*, 4212–4225. (b) Carter, C. W., Jr.; Kraut, J.; Freer, S. T.; Alden, R. A. *Ibid.* **1974**, *249*, 6339–6346. (c) Freer, S. T.; Alden, R. A.; Carter, C. W., Jr.; Kraut, J. *Ibid.* **1975**, *250*, 46–54.
(5) Ghosh, D.; O'Donnell, S.; Furey, W., Jr.; Robbins, A. H.; Stout, C. D. *J. Mol. Biol.* **1982**, *158*, 73–109.
(6) Berg, J. M.; Holm, R. H. In *Metal Ions in Biology*; Spiro, T. G., Ed.; Wiley-Interscience: New York, 1982; Vol. 4, Chapter 1.
(7) (a) Yang, C. Y.; Johnson, K. H.; Holm, R. H.; Norman, J. G., Jr. *J. Am. Chem. Soc.* **1975**, *97*, 6596–6598. (b) Thomson, A. J. *J. Chem. Soc., Dalton Trans.* **1981**, 1180–1189. (c) Aizman, A.; Case, D. A. *J. Am. Chem. Soc.* **1982**, *104*, 3269–3279. (d) Noodleman, L.; Norman, J. G., Jr.; Osborne, J. H., Aizman, A.; Case, D. A. *Ibid.* **1985**, *107*, 3418–3426.
(8) Sweeney, W. V. *Annu. Rev. Chem.* **1980**, *49*, 139–161.
(9) (a) DePamphilis, B. V.; Averill, B. A.; Herskovitz, T.; Que, L., Jr.; Holm, R. H. *J. Am. Chem. Soc.* **1974**, *96*, 4159–4167. (b) Mascharak, P. K.; Hagen, K. S.; Spence, J. T.; Holm, R. H. *Inorg. Chim. Acta* **1983**, *80*, 157–170.
(10) O'Sullivan, T.; Millar, M. *J. Am. Chem. Soc.* **1985**, *107*, 4096–4097.
(11) (a) Adman, E. T.; Watenpaugh, K. D.; Jensen, L. H. *Proc. Natl. Acad. Sci. U.S.A.* **1975**, *72*, 4854–4858. (b) Carter, C. W., Jr. In *Iron-Sulfur Proteins*; Lovenberg, W., Ed.; Academic: New York, 1977; Vol. 3, pp 157–206. (c) Sweeney, W. V.; Magliozzo, R. S. *Biopolymers* **1980**, *19*, 2133–2141. (d) Sheridan, R. P.; Allen, L. C.; Carter, C. W., Jr. *J. Biol. Chem.* **1981**, *256*, 5052–5057.
(12) (a) Stephan, D. W.; Papaefthymiou, G. C.; Frankel, R. B.; Holm, R. H. *Inorg. Chem.* **1983**, *22*, 1550–1557. (b) Hagen, K. S.; Watson, A. D.; Holm, R. H. *Ibid.* **1984**, *23*, 2984–2990.
(13) Averill, B. A.; Herskovitz, T.; Holm, R. H.; Ibers, J. A. *J. Am. Chem. Soc.* **1973**, *95*, 3523–3534.
(14) Que, L., Jr.; Bobvik, M. A.; Ibers, J. A.; Holm, R. H. *J. Am. Chem. Soc.* **1974**, *96*, 4168–4178.
(15) Christou, G.; Garner, C. D.; Drew, M. G. B.; Cammack, R. *J. Chem. Soc., Dalton Trans.* **1981**, 1550–1555.
(16) Carrell, H. L.; Glusker, J. P.; Job, R.; Bruice, T. C. *J. Am. Chem. Soc.* **1977**, *99*, 3683–3690.

0002-7863/87/1509-7178$01.50/0

$C_4H_9^-$,[9b] and Cl^-,[17] as terminal ligands. In all these cases the Fe_4S_4 cube is slightly flattened with four short and eight long Fe–S bonds. The bond length difference ranges from 0.02 to 0.07 Å. Recently, however, Kanatzidis et al.[18] have found that this D_{2d} distortion does not apply to $[Fe_4S_4]^{2+}$ compounds with mixed terminal ligands, Cl^- and SPh^- or OPh^-. Three examples of $[Fe_4S_4]^+$ have been examined, with SPh^-,[19] SCH_2Ph^-,[20] and S-*p*-$C_6H_4Br^-$[21] as terminal ligands. In the $[Fe_4S_4(SPh)_4]^{3-}$ cluster the Fe_4S_4 core is elongated with eight short and four long Fe–S bonds, the difference being 0.036 Å. Structures of the latter two are less regular. Holm et al.[19,21,22] have presented spectroscopic and magnetic evidence that $[Fe_4S_4(SCH_2Ph)_4]^{3-}$ and several other $[Fe_4S_4]^+$ containing clusters have the same, elongated core structure in solution. The apparent shift from a compressed to an elongated cube upon reduction of $[Fe_4S_4]^{2+}$ had been connected to possible Jahn–Teller activity, since early electronic structure calculations had given degenerate ground states for $[Fe_4S_4(SH)_4]^{2-}$ and $[Fe_4S_4(SCH_3)_4]^{2-}$.[7a] However, Thomson[7b] pointed out that the existing spectroscopic data indicate a nondegenerate ground state for the $[Fe_4S_4]^{2+}$ species, and recent calculations,[7c,d] involving more realistic model geometries than were used in the earlier calculations, predict that the ground state is indeed nondegenerate.

Several forms of spectroscopy have been fruitfully applied to the Fe_4S_4 clusters.[1] Among them resonance Raman (RR) spectroscopy is capable of providing detailed structural information via laser excitation in the strong visible region absorption bands, associated with S → Fe charge-transfer transitions. Since such transitions should weaken the Fe–S bonds in the excited electronic states, resonance enhancement is expected for Raman modes associated with Fe–S stretching vibrations.[23] Although the Fe–S protein rubredoxin was the object of one of the first biological applications of RR spectroscopy, in the pioneering study by Long and Loehr[24] over 15 years ago, progress has been slow[25] due to technical difficulties associated with photolability and the relatively modest resonance enhancement factors associated with Fe–S complexes. These obstacles have yielded to experimental advances in recent years, and good quality spectra have been reported for 1-Fe,[26] 2-Fe,[27] 3-Fe,[28] and 4-Fe[28b,d,e,29] centers.

If RR spectroscopy is to be properly utilized, the vibrational character of the observed modes must be understood. The present study is an analysis of the vibrational modes of $[Fe_4S_4]^{2+}$ clusters focussing particularly on $[Fe_4S_4(SCH_2Ph)_4]^{2-}$, "benzyl cube", as a model for the protein-bound clusters. RR spectra have been complemented with infrared spectra, which have yielded much useful data. ^{34}S substitution, in both cluster and terminal thiolate positions, has been used to assign the bands. Some of these assignments are in agreement with the recent suggestions of Moulis et al.,[29b] based on RR spectra of Fd and analogues, with ^{34}S and Se substitution, but others are not. A normal coordinate analysis, with Urey–Bradley force constants scaled from related molecules, has been used to obtain accurate normal mode compositions.

New high-quality RR spectra of Fd and HiPIP have been obtained and analyzed with reference to the benzyl cube assignments. They provide strong evidence that *Cp* Fd imposes a significant D_{2d} distortion on its Fe_4S_4 clusters while *Cv* HiPIP is less distorted. This difference may be an indicator of underlying protein forces that determine the very different redox properties of these proteins.

Materials and Methods

Proteins. Samples of reduced high-potential iron–sulfur protein from *Chromatium vinosum* (*Cv* HiPIP) and oxidized ferredoxin from *Clostridium pasteurianum* (*Cp* Fd) were kindly supplied by K. K. Rao (Kings College, London, U.K.) and M. W. W. Adams and T. V. Morgan (EXXON Research and Engineering Co., Annandale, NJ), respectively. The formation of *Cp* Fd apoprotein and subsequent reconstitution with isotopically labeled $^{34}S^{2-}$ was carried out as described in ref 28b. ^{34}S (95% isotopic purity, Oak Ridge National Laboratories) was converted to $Na_2{}^{34}S$ by reacting it with elemental Na in liquid ammonia.[30] ^{54}Fe insertion into *Cp* Fd was achieved by following the enzymic reconstitution procedure of Bonomi et al.,[31] except that $^{54}FeCl_3$ was used in place of ferric ammonium citrate, dithiothreitol replaced D,L-dihydrolipoate, and the reaction was carried out at pH 7.1 instead of pH 8.1. ^{54}Fe was purchased as $^{54}Fe_2O_3$ (97% isotopic purity) from Oak Ridge National Laboratories and converted to $^{54}FeCl_3$ by reacting it with concentrated HCl. The 390/280-nm absorbance ratios were 0.83 for both ^{34}S and ^{54}Fe reconstituted proteins. Electronic absorption spectra were recorded on a Hewlett Packard Model 8450 spectrophotometer.

Analogue Complexes. The $(Et_4N)_2[Fe_4S_4(SCH_2Ph)_4]$ complex was synthesized by a procedure similar to that of Christou and Garner,[32] using lithium dissolved in CH_3OH, phenylmethanethiol, $FeCl_2{\cdot}4H_2O$ dissolved in CH_3OH, elemental sulfur, and Et_4NI dissolved in CH_3OH. All manipulations were carried out under a purified N_2 atmosphere in Schlenk-type apparatus. Reagent grade methanol was carefully purged with N_2 and degassed with 4 freeze–pump–thaw cycles; no attempt was made to remove trace amounts of water.[32] The analogues with ^{34}S at either bridging or terminal positions were prepared by the same procedure, using the elemental ^{34}S or the ligand $C_6H_5CH_2{}^{34}SH$. $C_6H_5CH_2{}^{34}SH$ was prepared from Grignard reagent, $C_6H_5CH_2MgCl$ (Aldrich Chemical Co.), and elemental ^{34}S according to a published method.[33] ^{34}S (90% isotopic enrichment) was purchased from Monsanto Research Corp.

Infrared and Resonance Raman Spectroscopy. Infrared spectra of analogue complexes were obtained with a Digilab FT20C Fourier transform infrared spectrophotometer equipped with a N_2 purge sample chamber. In a O_2-free drybox, approximately 15 mg of sample was ground with 1 drop of Nujol to form a mull

(17) Bobvik, M. A.; Hodgson, K. O.; Holm, R. H. *Inorg. Chem.* **1977**, *16*, 1851–1858.
(18) Kanatzidis, M. G.; Baenziger, N. C.; Coucouvanis, D.; Simopoulos, A.; Kos, A. *J. Am. Chem. Soc.* **1984**, *106*, 4500–4511.
(19) Laskowski, E. J.; Frankel, R. B.; Gillum, W. O.; Papaefthymiou, G. C.; Renaud, J.; Ibers, J. A.; Holm, R. H. *J. Am. Chem. Soc.* **1978**, *100*, 5322–5337.
(20) Berg, J. M.; Hodgson, K. O.; Holm, R. H. *J. Am. Chem. Soc.* **1979**, *101*, 4586–4593.
(21) Stephan, D. W.; Papaefthymiou, G. C.; Frankel, R. B.; Holm, R. H. *Inorg. Chem.* **1983**, *22*, 1550–1557.
(22) Laskowski, E. J.; Reynolds, J. G.; Frankel, R. B.; Foner, S.; Papaefthymiou, G. C.; Holm, R. H. *J. Am. Chem. Soc.* **1979**, *101*, 6562–6570.
(23) Spiro, T. G.; Hare, J.; Yachandra, V.; Gewirth, A.; Johnson, M. K.; Remsen, E. In *Metal Ions in Biology*; Spiro, T. G., Ed.; Wiley-Interscience: New York, 1982; Vol. 4, Chapter 6.
(24) Long, T. v.; Loehr, T. M. *J. Am. Chem. Soc.* **1970**, *92*, 6384–6386.
(25) (a) Long, T. V.; Loehr, T. M.; Allkins, J. R.; Lovenberg, W. *J. Am. Chem. Soc.* **1971**, *93*, 1809–1811. (b) Tang, S. P. W.; Spiro, T. G.; Mukai, K.; Kimura, T. *Biochem. Biophys. Res. Commun.* **1973**, *53*, 869–874. (c) Tang, S. P. W.; Spiro, T. G.; Antanaitis, C.; Moss, T. M.; Holm, R. H.; Herskovitz, T.; Mortenson, L. E. *Ibid.* **1975**, *62*, 1–6. (d) Blum, H.; Adar, F.; Salerno, J. C.; Leigh, J. C., Jr. *Ibid.* **1977**, *77*, 650–657. (e) Adar, F.; Blum, H.; Leigh, J. S., Jr.; Ohnishi, T.; Salerno, J. C.; Kimura, J. *FEBS Lett.* **1977**, *84*, 214–216.
(26) (a) Yachandra, V. K.; Hare, J.; Moura, I.; Spiro, T. G. *J. Am. Chem. Soc.* **1983**, *105*, 6455–6461. (b) Czernuszewicz, R. S.; LeGall, J.; Moura, I.; Spiro, T. G. *Inorg. Chem.* **1986**, *25*, 696–700.
(27) (a) Yachandra, V. K.; Hare, J.; Gewirth, A.; Czernuszewicz, R. S.; Kimura, T.; Holm, R. H.; Spiro, T. G. *J. Am. Chem. Soc.* **1983**, *105*, 6462–6468. (b) Ozaki, Y.; Nagayama, K.; Kyogoku, Y.; Hase, T.; Matsubara, *FEBS Lett.* **1982**, *152*, 236–240. (c) Meyer, J.; Moulis, J.-M.; Lutz, M. *Biochem. Biophys. Res. Commun.* **1984**, *119*, 828–835.
(28) (a) Johnson, M. K.; Hare, J. W.; Spiro, T. G.; Moura, J. J. G.; Xavier, A. V.; LeGall, J. *J. Biol. Chem.* **1981**, *256*, 9806–9808. (b) Johnson, M. K.; Spiro, T. G.; Mortensen, L. E. *Ibid.* **1982**, *257*, 2447–2452. (c) Johnson, M. K.; Czernuszewicz, R. S.; Spiro, T. G.; Ramsay, R. R.; Singer, T. P. *Ibid.* **1983**, *258*, 12771–12774. (d) Johnson, M. K.; Czernuszewicz, R. S.; Spiro, T. G.; Fee, J. A.; Sweeney, W. V. *J. Am. Chem. Soc.* **1983**, *105*, 6671–6678. (e) Lutz, M.; Moulis, J.-M.; Meyer, J. *FEBS Lett.* **1983**, *163*, 212–216.
(29) (a) Moulis, J.-M.; Meyer, J.; Lutz, M. *Biochem. J.* **1984**, *219*, 829–832. (b) Moulis, J.-M.; Meyer, J.; Lutz, M. *Biochemistry* **1984**, *23*, 6605–6613.
(30) Brauer, G. *Handbook of Preparative Inorganic Chemistry*; Academic: New York, 1963; Vol. 1, pp 358–360.
(31) Bonomi, F.; Pagani, S.; Kurtz, D. M., Jr. *J. Biochem.* **1985**, *148*, 67–73.
(32) Christou, G.; Garner, C. D. *J. Chem. Soc., Dalton Trans.* **1979**, 1093–1094.
(33) Wardell, J. L. In *The Chemistry of the Thiol Group*, Part I; Patai, S., Ed.; Wiley: New York, 1974; pp 211–215.

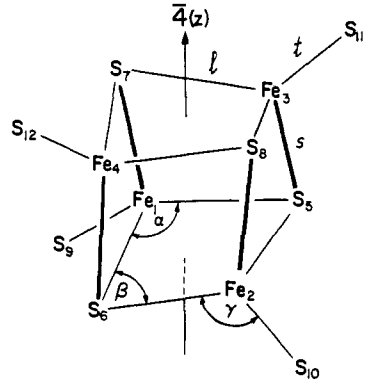

Figure 1. Structure and internal coordinates for the $Fe_4S_4{}^bS_4{}^t$ cube of $(Et_4N)_2[Fe_4S_4(SCH_2Ph)_4]$. Bond distances, t = 2.251 Å, l = 2.310 Å, and s = 2.239 Å; angles, α = 104.2°, β = 73.9° , and γ = 114.1°; and nonbonded distances, $Fe_1\cdots Fe_2$ = $Fe_3\cdots Fe_4$ = 2.776 Å and $S_5\cdots S_6$ = $S_7\cdots S_8$ = 3.645 Å, taken from ref 13, were used for normal mode calculations.

which was spread between 0.5 mm thick polyethylene plates (1 cm in diameter) and placed in a Cu holder. The holder was fastened to a cold finger and inserted in an evacuated shroud with 1 mm thick polyethylene windows (2 cm in diameter).

In our experience, the best technique for obtaining Fe–S resonance Raman spectra is backscattering from the surface of a frozen solution (proteins) or a KCl pellet (analogue complexes) kept in a liquid-N_2 dewar.[34] Under these conditions no sample damage was observed, even during prolonged (~6–12 h) spectral data acquisition at laser power levels of ~200–400 mW. In addition, this technique eliminates interference from glass or quartz scattering, since the samples require no covering.[34] The protein samples (~2 mM) were in 0.05 M Tris–HCl buffer, pH 7.5. The solid samples (~2–3 mg) were ground with ~100 mg of KCl powder and pressed into 7-mm-diameter pellets by a KBr Pellet Grip Press (Jones Technology, Townshead, VT). Preparation and mounting of the pellets onto a cold finger were performed in the O_2-free drybox. To ensure accurate determination of isotope shifts, isotopic and natural abundance samples were affixed in pairs on the cold finger, and the dewar was accurately positioned in the sample compartment of the Raman spectrometer through the use of an x,y,z-translation stage, allowing the two RR spectra to be recorded under the same conditions.

The analogue complex solution for low-temperature RR measurements was prepared in the O_2-free drybox by dissolving $(Et_4N)_2[Fe_4S_4(SCH_2Ph)_4]$ in an aqueous detergent medium[35] consisting of 90/5/5 (vol %) H_2O/*N,N*-dimethylacetamide (DMA)/Triton X-100. Room temperature RR spectra of $(Et_4N)_2[Fe_4S_4(SCH_2Ph)_4]$ and its ^{34}S analogues (~5 mM in DMA) were obtained by backscattering from sealed NMR tubes cooled with cold N_2 gas.[36]

Exciting radiation for RR spectra was provided by Coherent Radiation CR-5 Ar^+ (454.5–514.5 nm) and Spectra Physics 171 Kr^+ (406.7, 413.1 nm) ion lasers. The scattered radiation was dispersed by a Spex 1401 double monochromator and detected by a cooled RCA 31034A photomultiplier tube with an ORTEC 9315 photoncounting system, under the control of a MINC II (DEC) minicomputer. Polarization measurements were carried out on the solid samples[37] (KCl pellet) by analyzing the scattered light (180°) in front of the monochromator slit.

Normal Coordinate Calculations. Normal mode calculations were performed by using the GF matrix method[38] and a Urey–Bradley force field. Molecular parameters were obtained from the crystal structure data[13] from which Cartesian coordinates were determined via simple trigonometric relationships developed by holding bond lengths and Fe–Fe and S–S distances constant to maintain D_{2d} symmetry. Comparison of actual nonbonded distances with those calculated in this geometry showed deviations of no more than 0.01 Å. Schachtschneider's programs[39] were used for constructing G matrices and solving the secular equations.

Table I. Symmetry Lowering and Spectroscopic Activity[a]

T_d	—	D_{2d}
A_1 (R)	—	A_1 (R)
E (R)	<	A_1 (R)
		B_1 (R)
T_1 (i.a.)	<	A_2 (i.a.)
		E (R, IR)
T_2 (R, IR)	<	B_2 (R, IR)
		E (R, IR)

[a] R, Raman active; IR, infrared active; i.a., inactive in IR or nonresonance Raman—these modes have antisymmetric scattering tensors ($\alpha_{jl} = -\alpha_{lj}$), however, and can be activated via vibronic coupling in resonance with the coupled electronic transitions.

Results and Discussion

Cluster Mode Structure and Symmetry: Assignments for Benzyl Cube. The basic four-iron cluster under consideration is shown schematically in Figure 1. Structure parameters for $(Et_4N)_2[Fe_4S_4(SCH_2Ph)_4]$ are listed in the caption. The molecular symmetry conforms closely to D_{2d}, as it does for several $[Fe_4S_4]X_4^{2-}$ clusters,[6] with four short and eight long Fe–S bridge bonds; those are labeled s and l in Figure 1, and in subsequent tables. The structure is not far from T_d symmetry, however, and the vibrational spectra are usefully interpreted via the descent from T_d to D_{2d} symmetry. As will be seen the spectra indicate very little if any symmetry lowering for benzyl cube in solution. Table I gives a $T_d \rightarrow D_{2d}$ correlation table.

If the thiolate ligands are treated as points the vibrational modes of a T_d $(Fe_4S_4{}^b)S_4{}^t$ fragment classify as

$$\Gamma_{vib} = 3A_1 + 3E + 2T_1 + 5T_2$$

Contributions from the various internal coordinates to these modes, and to their D_{2d}-associated components, are given in Table II. We are mainly concerned with Fe–S stretching modes, observed in the 240–400-cm^{-1} region. The twelve Fe–S^b bonds in the Fe_4S_4 core give rise to five T_d stretching modes

$$\Gamma_{FeS^b} = A_1 + E + T_1 + 2T_2$$

while the terminal Fe–S^t bonds give rise to two T_d modes

$$\Gamma_{FeS^t} = A_1 + T_2$$

The remaining modes are associated with FeS deformations and occur at lower frequencies. They are expected to be weak in both Raman and IR spectra. Fe–S^t deformations span the representations $E + T_1 + T_2$, while $Fe_4S_4{}^b$ deformations span $A_1 + E + T_2$. These last three modes can be described in terms of displacements of the Fe–Fe (or S–S) interactions, or of the internal cube angles, these coordinate sets being completely redundant (see Table II). RR spectra of benzyl cube, and also of *Cp* ferredoxin, show a weak band at 165 cm^{-1} (not shown), which is probably the A_1 breathing mode of the Fe_4 tetrahedron. This is the only band in the ~200-cm^{-1} region, where metal–metal frequencies are expected.[40] For example, the Fe_4 breathing mode of $[(C_5H_5)Fe(CO)]_4$ has been assigned at 214 cm^{-1}.[41] While the Fe–Fe contacts, ~2.75 Å,[2,6] are moderately short and the Fe spins are antiferromagnetically coupled, there is no reason to think that direct bonding between the Fe atoms is energetically important.

(34) Czernuszewicz, R. S.; Johnson, M. K. *Appl. Spectrosc.* **1983**, *37*, 297–298.
(35) Stevens, W. C.; Kurtz, D. M., Jr. *Inorg. Chem.* **1985**, *24*, 3444–3449.
(36) Walters, M. A. *Appl. Spectrosc.* **1983**, *37*, 299–301.
(37) na) Strommen, D. P.; Nakamoto, K. *Appl. Spectrosc.* **1983**, *37*, 436–439. (b) Strommen, D. P.; Bajdor, K.; Czernuszewicz, R. S.; Blinn, E. L.; Nakamoto, K. *Inorg. Chim. Acta* **1982**, *63*, 151–155.
(38) Wilson, E. B.; Decius, J. C.; Cross, P. C. *Molecular Vibrations*; McGraw-Hill: New York, 1955.
(39) Schachtschneider, J. H. Shell Development Co., Technical Report No. 263-263, 1962.
(40) Spiro, T. G. *Prog. Inorg. Chem.* **1970**, *11*, 1–51.
(41) Terzis, A.; Spiro, T. G. *Chem. Commun.* **1970**, 1160–1161.

Table II. $Fe_4S^b_4S^t_4$ Normal Mode Classification

internal coordinate	no. of contributions to each symmetry class; T_d symmetry			
	A_1	E	T_1	T_2
terminal				
Fe–S^t bond stretch (4)	1			1
S^b–Fe–S^t angle bend (12)	(1)	1	1	1 + (1)
cube				
Fe–S^b bond stretch (12)[a]	1	1	1	2
Fe-Fe bond stretch (6)	1	1		1
Fe–S^b–Fe angle bend (12)	(1)[b]	(1)	(1)	(2)
S^b–Fe–S^b angle bend (12)	(1)	(1)	(1)	(2)

	no. of contributions to each symmetry class; D_{2d} symmetry						
	A_1	A_1	B_1	A_2	E	B_2	E
terminal							
t, Fe–S^t bond stretch (4)	1					1	1
λ_{ts}, S^b–Fe–St angle bend (4)	(1)					1	1
λ_{tl}, S^b–Fe–S^t angle bend (8)		1	1	1	1	(1)	(1)
cube							
l, Fe–S^b long bond stretch (8)		1	1	1	1	1	1
s, Fe–S^b short bond stretch (4)	1					1	1
Fe–Fe short bond stretch (4)		1	1			1	1
Fe–Fe long bond stretch (2)	1					1	
β_{sl}, Fe–S^b–Fe angle bend (8)		(1)	(1)	(1)	(1)	(1)	(1)
β_{ll}, Fe–S^b–Fe angle bend (4)	(1)					(1)	(1)
α_{sl}, S^b–Fe–S^b angle bend (8)		(1)	(1)	(1)	(1)	(1)	(1)
α_{ll}, S^b–Fe–S^b angle bend (4)	(1)					(1)	(1)

[a] Numbers in parentheses indicate the number of coordinates in each group. S^b and S^t refer to bridging and terminal sulfur, respectively. [b] ( ) denotes redundancy.

The weakness of the 165 cm^{-1} band indicates that there is no large change in the Fe–Fe distances between the ground and excited states.

All of the Fe–S stretching modes are assignable in the RR and IR spectra of solid $(Et_4N)_2[Fe_4S_4(SCH_2Ph)_4]$, with the aid of ^{34}S isotope shifts, on the basis of descent from T_d to D_{2d} symmetry. The IR spectra are shown in Figure 2. Three T_2 modes are expected and are readily observed at 243/250, 359/366, and 386 cm^{-1}, the first two showing the expected splitting into two components (E and B_2). The 243/250- and 386-cm^{-1} bands show 4–6-cm^{-1} $^{34}S^b$ shifts and are assigned to the two expected Fe–S^b T_2 modes. Similarly large $^{34}S^t$ shifts are seen for the 359/366-cm^{-1} doublet, which is assigned to the single Fe–S^t T_2 mode. Its high IR intensity can be understood on the basis of the large dipole generated by the stretching of Fe–S^t bonds across the Fe_4 tetrahedron. The D_{2d} selection rules allow IR activity for the E component of the T_1 Fe–S^b mode, but since the parent mode is inactive in T_d symmetry the intensity is expected to be low. No candidate band is found in the IR spectra. Neither the T_d E mode nor its A_1 and B_1 D_{2d} components are IR active. The remaining bands in the IR spectrum, at 267, 320, 331, 471, and 477 cm^{-1}, have correspondences in the IR spectrum of the benzyl thiolate itself (not shown) and are ascribed to internal ligand modes. Turning to the RR spectrum of solid $(Et_4N)_2[Fe_4S_4(SCH_2Ph)_4]$, shown in Figure 3, we readily locate the three T_2 modes at 243/249, 359/367, and 385 cm^{-1} via their selective $^{34}S^b$ shifts and their coincidence with the previously assigned IR bands. The strongest RR band, at 335 cm^{-1}, shifts 8 cm^{-1} on $^{34}S^b$ substitution and is assigned to the A_1 Fe–S^b stretch, which is the cube breathing mode. The next strongest band, at 391 cm^{-1}, shows only a 1-cm^{-1} $^{34}S^b$ shift and is assigned to the A_1 Fe–S^t stretch.

There remain three $^{34}S^b$-sensitive RR bands, 270, 283, and 298 cm^{-1}, which must rise from components of the E and T_1 Fe–S^b modes. In T_d symmetry the E mode is Raman active and depolarized, while its D_{2d} components, A_1 and B_1, are polarized and depolarized, respectively. The T_1, which transforms as molecular rotations, has an antisymmetric scattering tensor and is active only under resonance conditions, where it should exhibit inverse polarization. In D_{2d} symmetry the T_1 components are E (depolarized) and A_2 (inverse polarized). Figure 4 shows polarization measurements for the low-temperature RR spectra of the solid $(Et_4N)_2[Fe_4S_4(SCH_2Ph)_4]$. Although the polarization is partially scrambled by multiple scattering from polycrystalline materials,

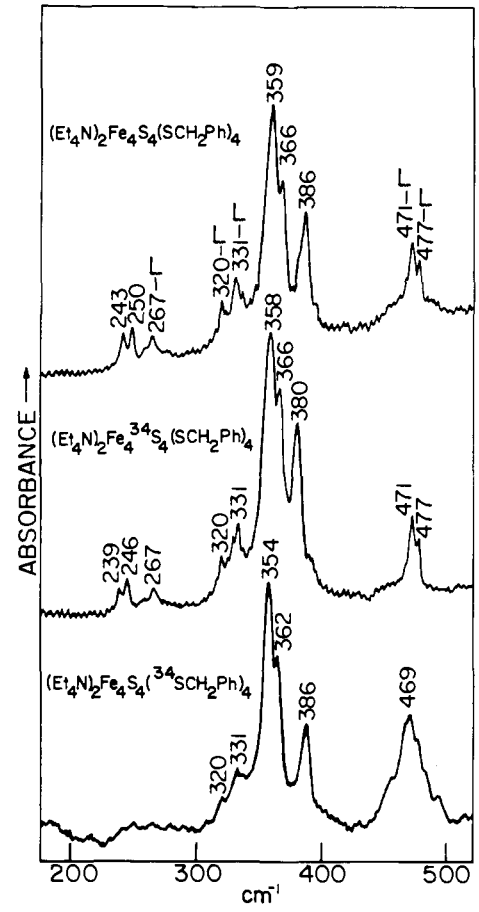

Figure 2. Low-temperature (77 K) infrared spectra of $(Et_4N)_2[Fe_4S_4(SCH_2Ph)_4]$ and its ^{34}S derivatives obtained with a Digilab FTIR, on Nujol mulls sealed between polyethylene plates. "L" marks bands associated with internal modes of $PhCH_2S^-$ ligand and Et_4N^+ counterion.

this effect is minimized when the sample absorbs strongly, and appreciable polarization remains,[37] for which symmetry labels can still be deduced, as Lutz and co-workers have emphasized.[29b] The strongly polarized character of the A_1 modes at 335 and 391 cm^{-1}

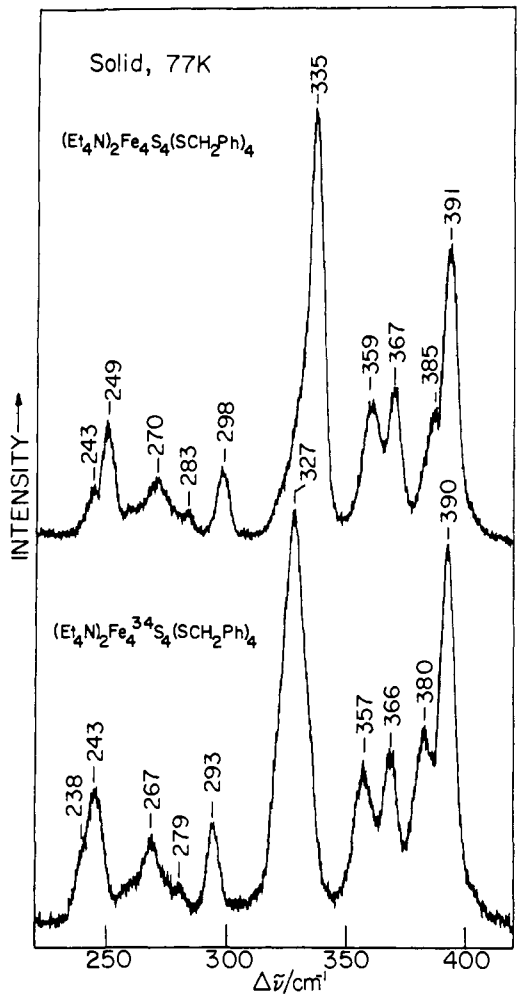

Figure 3. Resonance Raman spectra of $(Et_4N)_2[Fe_4S_4(SCH_2Ph)_4]$ and its $^{34}S^b$ isotope analogue in KCl pellet obtained via backscattering from a liquid-N_2 dewar with 5145 Å Ar^+ laser excitation (300 mW) and 4 cm^{-1} slit widths. For these data the spectrometer was advanced in 0.2-cm^{-1} increments at 2 s per point.

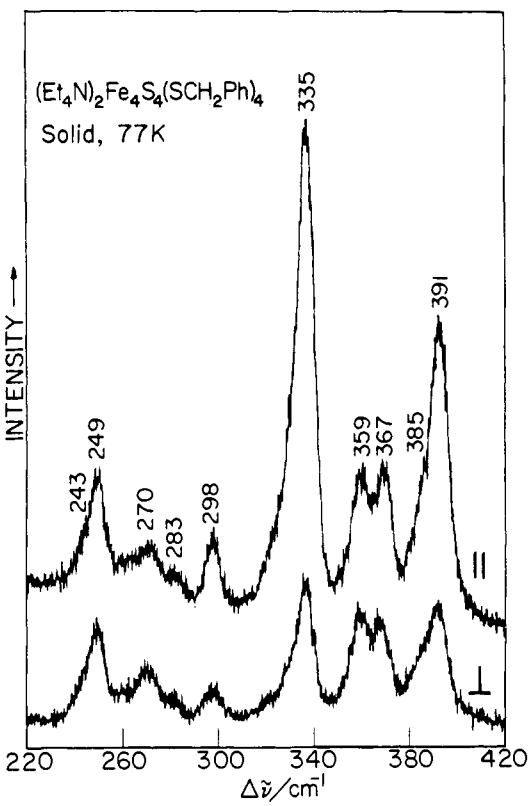

Figure 4. Low-temperature (77 K) Raman spectra in parallel and perpendicular polarizations obtained with 5145 Å Ar^+ laser excitation and 7 cm^{-1} slit widths, while the spectrometer was advanced in 0.2-cm^{-1} increments.

is evident, and the new 298-cm^{-1} band is also seen to be polarized. It is therefore assigned to the A_1 component of the E mode. The remaining bands are largely depolarized, as expected, except that the 270-cm^{-1} band appears to have stronger perpendicular than parallel scattering. On this basis it is assigned to the A_2 component of the T_1 mode. The remaining band, at 283 cm^{-1}, can be either the $B_1(E)$ of the $E(T_1)$ component, or both.

These assignments are listed in Table IV.

Normal Coordinate Analysis. Normal coordinate calculations, using symmetry coordinates listed in Table III, were performed to test the reasonableness of the mode assignments and to examine the nature of the normal modes. A Urey–Bradley force field was employed, since it seems likely that nonbonded interactions among the sulfur atoms, and also among the Fe atoms, are important in the cluster structure. It was found empirically, however, that the numerical values of the nonbonded force constants had to be set substantially lower than might be expected on the basis of Urey–Bradley calculations on simple tetrahedral complexes,[42] such as $FeCl_4^-$; otherwise the correct values of the ^{34}S isotope shifts could not be obtained. No doubt, this lack of transferability reflects the inadequacy of a simple force field in describing the actual bonding situation in a cluster compound. From an empirical point of view, however, it is satisfying that quite accurate results could be obtained with small values of the nonbonded constants, and without any need to invoke valence interaction constants. The primary force constants for stretching of the FeS bonds and bending the angles were taken from our previous work on FeS complexes[26a,27b] and adjusted slightly to give the best fit to the observed frequencies and isotope shifts. The force field was restricted, however, by using Badger's rule[43] ($K \propto (r - 1.02)^{-3}$, where r is the bond length) to fix the ratio of the stretching force constants corresponding to the long and short Fe–S^b bonds within the D_{2d} cluster. In addition the nonbonded force constants for different pairs of S atoms and Fe atoms were constrained to a d^{-9} distance dependence.[44]

The results of the calculation are given in Table IV. Observed and calculated frequencies agree to within 1 cm^{-1} except for the group of T_1 and E (T_d) mode components, where discrepancies are less than 7 cm^{-1}. Even more important, the $^{34}S^b$ isotope shifts agree with the calculations to within 0.9 cm^{-1}. Also in excellent agreement (0.4 cm^{-1}) are the calculated and observed ^{54}Fe shifts (Table IV). The latter were obtained via ^{54}Fe reconstitution of *Cp* Fd, whose RR spectrum is very similar to that of solid $(Et_4N)_2[Fe_4S_4(SCH_2Ph)_4]$ (vide infra). The only discrepancy is the $A_2(T_1)$ component for which the observed ^{54}Fe shift is only 0.4 cm^{-1}, while 2.3 cm^{-1} is expected. We believe the observed shift may be artificially low due to a near coincidence with an internal mode of the cysteinate ligands, analogous to the internal ligand mode observed in the IR spectrum of $(Et_4N)_2[Fe_4S_4(SCH_2Ph)_4]$ at 268 cm^{-1} (Figure 2). Since the ligand mode would not be ^{54}Fe sensitive the apparent shift would be less than the actual shift of the Fe–S^b mode. Although the ^{54}Fe shifts do not discriminate between terminal and bridging modes, as the ^{34}S shifts do, they provide an additional sensitive check on the calculations, which are seen to give a very satisfactory account of the Fe–S stretching modes. Although the agreement with observation cannot be taken as proof that the force field is correct, the accurate calculation of isotope shifts does imply that the calculated eigenvectors are

(42) Avery, J. S.; Burbridge, C. D.; Goodgame, D. M. L. *Spectrochim. Acta* **1968**, *24A*, 1721–1726.

(43) (a) Badger, R. M. *J. Chem. Phys.* **1934**, *2*, 128–131. (b) Badger, R. M. *J. Chem. Phys.* **1935**, *3*, 710–714. (c) Hershbach, D. R.; Laurie, V. W. *J. Chem. Phys.* **1961**, *35*, 458–462.

(44) Nakamoto, K. *Infrared and Raman Spectra of Inorganic and Coordination Compounds*; Wiley-Interscience: New York, 1986.

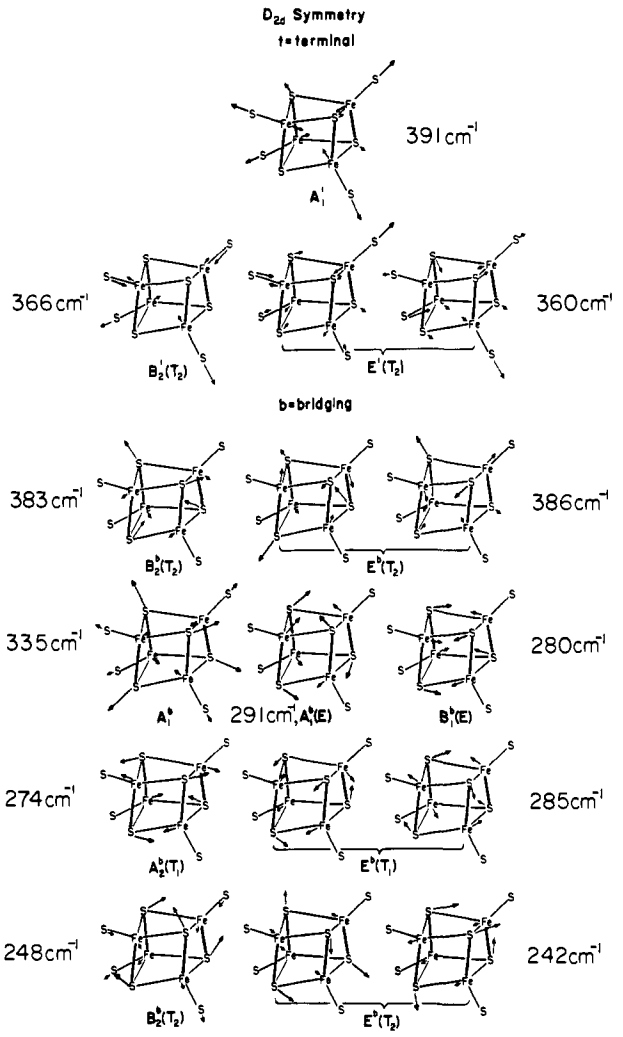

Figure 5. Normal modes of vibration of elongated (D_{2d} symmetry) $Fe_4S_4{}^bS^t$ cube.

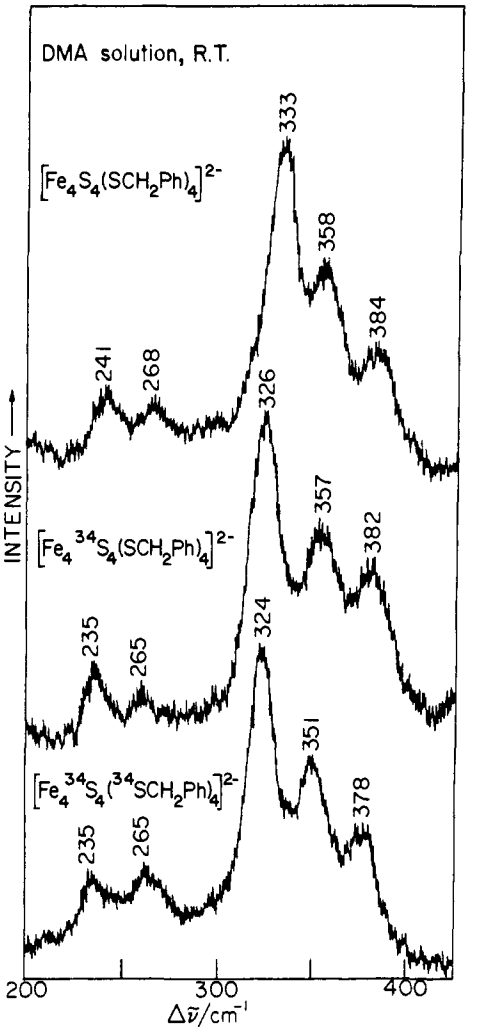

Figure 6. Room temperature resonance Raman spectra of $(Et_4N)_2[Fe_4S_4(SCH_2Ph)_4]$ and its ^{34}S derivatives obtained via backscattering on ≈5 mM solutions in diamethylacetamide, contained in sealed spinning NMR tubes cooled with cold N_2 gas; 4579 Å Ar^+ laser excitation, ~250 mW, 5 cm^{-1} slit widths. For these data the spectrometer was advanced in 0.5-cm^{-1} increments at 2 s per point.

good approximations to the normal modes. These are illustrated in Figure 5. Table IV gives potential energy contributions from the stretching coordinates for terminal and bridging (long and short) Fe–S bonds. We note that there is substantial mixing of terminal and bridging coordinates in the two $A_1(T_d)$ breathing modes (40% Fe–S^b in the mainly Fe–S^t 391-cm^{-1} mode, and 19% Fe–S^t in the mainly Fe–S^b 335-cm^{-1} mode) despite the large disparity in $^{34}S^b$ shifts.

We note that the Fe_4S_4 assignments suggested by Moulis et al.[29b] are in accord with ours for some modes but not others. Thus they assigned both T_2 Fe–S^t components to 353 cm^{-1} and the A_1 Fe–S^t mode to 365 cm^{-1}, instead of 391 cm^{-1}. Also the ordering of the Fe–S^t mode below 330 cm^{-1} is not in accord with the present ordering.

Benzyl Cube Is Tetrahedral in Solution. Figure 6 shows RR spectra of benzyl cube and its $^{34}S^b$ and $^{34}S^t$ isotopomers in *N,N*-dimethylacetamide solution. Although there is an overall similarity with the RR spectra of solid $(Et_4N)_2[Fe_4S_4(SCH_2Ph)_4]$ (Figure 3), including the same separation into terminal and bridging modes on the basis of the isotope shifts, there are also clear differences. The most obvious of these are (a) the intensity loss of the 391-cm^{-1} A_1 Fe–S_t stretch, (b) the collapse of the 359/367-cm^{-1} T_2 mode splitting, and (c) the loss of the 298-cm^{-1} $A_1(E)$ mode.

The deenhancement of the 391-cm^{-1} A_1 mode appears to be accompanied by a ~7-cm^{-1} frequency downshift. The broad 384-cm^{-1} solution band clearly contains overlapping contribution from the A_1 Fe–S^t and T_2 Fe–S^b modes, since it shifts on $^{34}S^t$ as well as $^{34}S^b$ substitution. In fact, the $^{34}S^t$ shift is larger (4 vs 2 cm^{-1}), indicating a greater Fe–S^t contribution. A possible source of the difference between solid and solution samples is the greater conformational flexibility of the thiolate ligands in solution. The Fe–S^t modes are expected to couple to some extent to internal modes of the thiolate ligand, especially the S–C–C bend. This question has been analyzed in some detail for 1-Fe protein rubredoxin and its analogues.[26a] The coupling depends on ligand orientation, especially the Fe–S–C–C dihedral angle. This ligand orientation is fixed in the crystalline solid, but there is free rotation about Fe–S and C–C bonds in solution.

It is conceivable that the conformational relaxation also accounts for the collapse of the T_2 Fe–S^t components, at 359 and 367 cm^{-1} in the solid, to a single band at 358 cm^{-1} in solution. The 367-cm^{-1} $B_2(T_2)$ component of the solid might lose intensity and/or shift down in frequency in solution, just as the A_1 Fe–S^t mode appears to do. On the other hand, it is important to note that the splitting of the T_2 modes is accurately reproduced in the normal mode calculation without any consideration of ligand mode coupling or conformational effects. Table IV shows that a good fit to the solution frequencies and isotope shifts is obtained with a T_d force field very similar to the one used for the D_{2d} calculations. The only changes between the T_d and D_{2d} force fields are a slight increase of the Fe–S^b stretching force constant associated with the short bands and a slight decrease in the S···S and Fe···Fe nonbonded constants associated with the long bonds. There is no change in the Fe–S^t force constant, yet the relatively large splitting of the Fe–S^t T_2 mode, 359/367 cm^{-1}, is satisfactorily reproduced. Thus, the observed splittings are consistent with a T_d structure in solution derived by relaxing the D_{2d} structure in

Table III. Symmetry Coordinates for the $Fe_4S^b_4S^t_4$ Cube in D_{2d} Symmetry

A_1 Species	
$S_1 = 1/\sqrt{8}[\Delta l(1,5) + \Delta l(3,7) + \Delta l(2,6) + \Delta l(4,8) + \Delta l(2,5) + \Delta l(3,8) + \Delta l(1,6) + \Delta l(4,7)]$[a]	$\nu(Fe-S^b)_l$[b]
$S_2 = 1/2[\Delta s(1,7) + \Delta s(3,5) + \Delta s(2,8) + \Delta s(4,6)]$	$\nu(Fe-S^b)_s$
$S_3 = 1/2[\Delta t(1,9) + \Delta t(2,10) + \Delta t(3,11) + \Delta t(4,12)]$	$\nu(Fe-S^t)_t$
$S_4 = 1/\sqrt{8}[\Delta\beta(1,7,3) + \Delta\beta(1,5,3) + \Delta\beta(2,8,4) + \Delta\beta(2,6,4) + \Delta\beta(2,8,3) + \Delta\beta(2,5,3) + \Delta\beta(1,7,4) + \Delta\beta(1,6,4)]$	$\delta(Fe-S^b-Fe)_{sl}$
$S_5 = 1/2[\Delta\beta(3,7,4) + \Delta\beta(1,6,2) + \Delta\beta(3,8,4) + \Delta\beta(1,5,2)]$	$\delta(Fe-S^b-Fe)_{ll}$
$S_6 = 1/\sqrt{8}[\Delta\gamma(7,3,11) + \Delta\gamma(6,2,10) + \Delta\gamma(8,4,12) + \Delta\gamma(5,1,9) + \Delta\gamma(8,3,11) + \Delta\gamma(5,2,10) + \Delta\gamma(7,4,12) + \Delta\gamma(6,1,9)]$	$\delta(S^b-Fe-S^t)_{lt}$
$S_7 = 1/2[\Delta\gamma(5,3,11) + \Delta\gamma(8,2,10) + \Delta\gamma(6,4,12) + \Delta\gamma(7,1,9)]$	$\delta(S^b-Fe-S^t)_{st}$
A_2 Species	
$S_8 = 1/\sqrt{8}[\Delta l(1,5) - \Delta l(3,7) + \Delta l(2,6) - \Delta l(4,8) - \Delta l(2,5) + \Delta l(3,8) - \Delta l(1,6) + \Delta l(4,7)]$	$\nu(Fe-S^b)_l$
$S_9 = 1/\sqrt{8}[\Delta\beta(1,7,3) - \Delta\beta(1,5,3) + \Delta\beta(2,8,4) - \Delta\beta(2,6,4) - \Delta\beta(2,8,3) + \Delta\beta(2,5,3) - \Delta\beta(1,7,4) + \Delta\beta(1,6,4)]$	$\delta(Fe-S^b-Fe)_{sl}$
$S_{10} = 1/\sqrt{8}[\Delta\gamma(7,3,11) - \Delta\gamma(6,2,10) + \Delta\gamma(8,4,12) - \Delta\gamma(5,1,9) - \Delta\gamma(8,3,11) + \Delta\gamma(5,2,10) - \Delta\gamma(7,4,12) + \Delta\gamma(6,1,9)]$	$\delta(S^b-Fe-S^t)_{lt}$
B_1 Species	
$S_{11} = 1/\sqrt{8}[\Delta l(1,5) + \Delta l(3,7) + \Delta l(2,6) + \Delta l(4,8) - \Delta l(2,5) - \Delta l(3,8) - \Delta l(1,6) - \Delta l(4,7)]$	$\nu(Fe-S^b)_l$
$S_{12} == 1/\sqrt{8}[\Delta\beta(1,7,3) + \Delta\beta(1,5,3) + \Delta\beta(2,8,4) + \Delta\beta(2,6,4) - \Delta\beta(2,8,3) - \Delta\beta(2,5,3) - \Delta\beta(1,7,4) - \Delta\beta(1,6,4)]$	$\delta(Fe-S^b-Fe)_{sl}$
$S_{13} = 1/\sqrt{8}[\Delta\gamma(7,3,11) + \Delta\gamma(6,2,10) + \Delta\gamma(8,4,12) + \Delta\gamma(5,1,9) - \Delta\gamma(8,3,11 - \Delta\gamma(5,2,10) - \Delta\gamma(7,4,12) - \Delta\gamma(6,1,9)]$	$\delta(S^b-Fe-S^t)_{lt}$
B_2 Species	
$S_{14} = 1/\sqrt{8}[\Delta l(1,5) - \Delta l(3,7) + \Delta l(2,6) - \Delta l(4,8) + \Delta l(2,5) - \Delta l(3,8) + \Delta l(1,6) - \Delta l(4,7)]$	$\nu(Fe-S^b)_l$
$S_{15} = 1/2[\Delta s(1,7) - \Delta s(3,5) + \Delta s(2,8) - \Delta s(4,6)]$	$\nu(Fe-S^b)_s$
$S_{16} = 1/2[\Delta t(4,12) - \Delta t(2,10) + \Delta t(3,11) - \Delta t(1,9)]$	$\nu(Fe-S^t)_t$
$S_{17} = 1/\sqrt{8}[\Delta\beta(1,7,3) - \Delta\beta(1,5,3) + \Delta\beta(2,8,4) - \Delta\beta(2,6,4) + \Delta\beta(2,8,3) - \Delta\beta(2,5,3) - \Delta\beta(1,7,4) + \Delta\beta(1,6,4)]$	$\delta(Fe-S^b-Fe)_{sl}$
$S_{18} = 1/2[\Delta\beta(3,7,4) - \Delta\beta(1,6,2) + \Delta\beta(3,8,4) - \Delta\beta(1,5,2)]$	$\delta(Fe-S^b-Fe)_{ll}$
$S_{19} = 1/\sqrt{8}[\Delta\gamma(7,3,11) - \Delta\gamma(6,2.10) + \Delta\gamma(8,4,12) - \Delta\gamma(5,1,9) + \Delta\gamma(8,3,11) - \Delta\gamma(5,2,10) + \Delta\gamma(7,4,12) + \Delta\gamma(6,1,9)]$	$\delta(S^b-Fe-S^t)_{lt}$
$S_{20} = 1/2[\Delta\gamma(5,3,11) - \Delta\gamma(8,2,10) + \Delta\gamma(6,4,12) - \Delta\gamma(7,1,9)]$	$\delta(S^b-Fe-S^t)_{st}$
E Species	
$^1S_{21} = 1/2[\Delta l(1,5) - \Delta l(2,6) + \Delta l(2,5) - \Delta l(1,6)]$ $^2S_{21} = 1/2[\Delta l(3,7) - \Delta l(4,8) + \Delta l(3,8) - \Delta l(4,7)]$	$\nu(Fe-S^b)_l$
$^1S_{22} = 1/2[\Delta l(1,5) - \Delta l(2,6) - \Delta l(2,5) + \Delta l(1,6)]$ $^2S_{22} = 1/2[\Delta l(3,7) - \Delta l(4,8) - \Delta l(3,8) + \Delta l(4,7)]$	$\nu(Fe-S^b)_l$
$^1S_{23} = 1/\sqrt{2}[\Delta s(1,7) - \Delta s(2,8)]$ $^2S_{23} = 1/\sqrt{2}[\Delta s(3,5) - \Delta s(4,6)]$	$\nu(Fe-S^b)_s$
$^1S_{24} = 1/\sqrt{2}[\Delta t(3,11) - \Delta t(4,12)]$ $^2S_{24} = 1/\sqrt{2}[\Delta t(1,9) - \Delta t(2,10)]$	$\nu(Fe-S^t)_t$
$^1S_{25} = 1/2[\Delta\beta(1,7,3) - \Delta\beta(2,8,4) + \Delta\beta(2,8,3) - \Delta\beta(1,7,4)]$ $^2S_{25} = 1/2[\Delta\beta(1,5,3) - \Delta\beta(2,6,4) + \Delta\beta(2,5,3) - \Delta\beta(1,6,4)]$	$\nu(Fe-S^b-Fe)_{sl}$
$^1S_{26} = 1/2[\Delta\beta(1,7,3) - \Delta\beta(2,8,4) - \Delta\beta(2,8,3) + \Delta\beta(1,7,4)]$ $^2S_{26} = 1/2[\Delta\beta(1,5,3) - \Delta\beta(2,6,4) - \Delta\beta(2,5,3) + \Delta\beta(1,6,4)]$	$\delta(Fe-S^b-Fe)_{sl}$
$^1S_{27} = 1/\sqrt{2}[\Delta\beta(3,7,4) - \Delta\beta(3,8,4)]$ $^2S_{27} = 1/\sqrt{2}[\Delta\beta(1,5,2) - \Delta\beta(1,6,2)]$	$\delta(Fe-S^b-Fe)_{ll}$
$^1S_{28} = 1/2[\Delta\gamma(5,1,9) - \Delta\gamma(6,2,10) + \Delta\gamma(5,2,10) - \Delta\gamma(6,1,9)]$ $^2S_{28} = 1/2[\Delta\gamma(7,3,11) - \Delta\gamma(8,4,12) + \Delta\gamma(8,3,11) - \Delta\gamma(7,4,12)]$	$\delta(S^b-Fe-S^t)_{lt}$
$^1S_{29} = 1/2[\Delta\gamma(5,1,9) - \Delta\gamma(6,2,10) - \Delta\gamma(5,2,10) + \Delta\gamma(6,1,9)]$ $^2S_{29} = 1/2[\Delta\gamma(7,3,11) - \Delta\gamma(8,4,12) - \Delta\gamma(8,3,11) + \Delta\gamma(7,4,12)]$	$\delta(S^b-Fe-S^t)_{lt}$
$^1S_{30} = 1/\sqrt{2}[\Delta\gamma(5,3,11) - \Delta\gamma(6,4,12)]$ $^2S_{30} = 1/\sqrt{2}[\Delta\gamma(7,1,9) - \Delta\gamma(8,2,10)]$	$\delta(S^b-Fe-S^t)_{st}$

[a] Symbols; l, s, t, α, β, and γ are internal coordinates defined in Figure 1. Numbers in parentheses refer to atoms connected by the internal coordinates, following the numbering system in Figure 1. [b] ν = stretching mode; γ = bending mode. S^b and S^t refer to bridging and terminal sulfurs, respectively. Subscripts s and l refer to short and long bridging Fe–S bonds, respectively. Subscript t refers to terminal Fe–S bonds.

the solid. But the evidence is equivocal because of the possible influence of ligand conformational effects. The solid-state splitting of the 243/249-cm^{-1} T_2 mode is small enough that it could be hidden in the 241-cm^{-1} solution band.

The disappearance of the 298-cm^{-1} band, however, is strong evidence that the solution structure is T_d. This band is the A_1 component of the cluster E mode, which involves elongation or compression of the cluster along a set of four parallel Fe–S^b bonds. It is this mode that carriers the cluster into the D_{2d} symmetry seen in the $(Et_4N)_2[Fe_4S_4(SCH_2Ph)_4]$ crystal structure. Although the E mode is formally Raman active it is not subject to resonance enhancement via the dominant A term mechanism,[45] which is limited to totally symmetric modes (A_1) along which the excited state potential is displaced. When the symmetry is lowered to D_{2d}, however, the E mode splits into B_1 and A_1 components. The A_1 component, being totally symmetric, is now subject to A-term enhancement. This accounts for the polarized 298-cm^{-1} band in the benzyl cube solid state spectrum. Its absence in solution implies a lack of distortion from T_d symmetry.

The initial finding of several ($Fe_4S_4^b$) structures all sharing a D_{2d} distortion led to the view that this distortion was an inherent feature of the cluster,[6] and early calculations provided a justification for this view by predicting an orbitally degenerate ground state, subject to Jahn–Teller (J–T) distortion.[7a] This conclusion was disputed by Thomson,[7b] who argued that the diamagnetic ground state of these species is unlikely to arise via a Jahn–Teller distortion. More recent theoretical calculations[7c,d] with more realistic structural parameters than the earlier ones predict a nondegenerate ground state, even in T_d symmetry. Kanatzidis et al.[18] have recently reported new $[(Fe_4S_4^b)X_2Y_2]^{2-}$ (X = SPh^-, Y = Cl^-, OPh^-, Br^-; X = OPh^-, Y = Cl^-) structures that do *not* show the usual division into four short and eight long Fe–S^b bonds, even though the structures do show deviations of the Fe_4S_4 core from T_d symmetry. There is evidently considerable plasticity in the Fe_4S_4 core, allowing it to accommodate steric influences associated with the ligand and with crystal packing, although the mean Fe–S^b distance stays close to 2.28 Å. The importance of crystal packing forces is shown by the structure of $[Fe_4S_4(S\text{-}t\text{-}$

(45) Spiro, T. G.; Stein, P. *Annu. Rev. Phys. Chem.* **1977**, *28*, 501–521.

Table IV. Observed and Calculated Fe–S Stretching Frequencies (cm^{-1}) and Isotope Shifts for Crystalline and Solution $(Et_4N)_2[Fe_4S_4(SCH_2Ph)_4]$

mode	crystalline state[a]		calcd[e]	$\Delta\nu_i(^{54}Fe-^{56}Fe)$[b]		PED (%)[c]			solution state[d]		
					calcd[e]		Fe–S^b			calcd[e]	mode
$D_{2d}(T_d)$	IR	RR	D_{2d}	RR	D_{2d}	Fe–S^t	*l*	*s*	RR	T_d	T_d
				Mainly Terminal ν(Fe–S)							
A_1		391 (1)[f]	391.3 (2.1)	3.0	3.3	59	21	19	384 (2)	389 (2)	A_1
$B_2(T_2)$	360 (0)	367 (1)	366.0 (0.8)	2.5	3.0	80		14	358 (1)	360 (2)	T_2
$E(T_2)$	359 (1)	359 (2)	360.0 (2.5)	2.6	2.5	60	18				
				Mainly Bridging ν(Fe–S)							
$B_2(T_2)$	386 (6)	385 (5)	383.0 (6.8)	1.9	2.1		44	35	384 (2)	379 (5)	T_2
$E(T_2)$			386.3 (5.2)	3.0	2.5	19	33	37			
A_1		335 (8)	335.1 (7.2)	0.3	0.5	19	26	30	333 (7)	333 (8)	A_1
$A_1(E)$		298 (5)	291.0 (4.3)	2.0	2.4		52	45	268 (3)	275 (4)	E
$B_1(E)$		283 (4)	280.3 (3.8)	2.2	2.4		99				
$E(T_1)$		283 (4)	285.4 (4.1)	2.2	2.4		48	44	268 (3)	273 (4)	T_1
$A_2(T_1)$		270 (3)	274.0 (3.9)	0.4	2.3		91				
$B_2(T_2)$	250 (4)	249 (6)	247.9 (5.3)	0.0	0.2		37	38	241 (6)	240 (6)	T_2
$E(T_2)$	243 (4)	243 (5)	242.4 (5.1)		0.4		67				

[a] IR (Nujol mull) and RR (KCl pellet) in crystalline state at low temperature (77 K). [b] Upshifts observed upon $^{54}Fe \rightarrow {}^{56}Fe$ substitution in *Cp* Fd_{ox} from RR spectra of frozen protein solutions (77 K). [c] Calculated potential energy distribution; percentage contributions are given for the stretching of Fe–S terminal and bridge bonds, the latter divided into long (*l*) and short (*s*) bond contributions for the D_{2d} structure. [d] RR in *N,N*-dimethylacetamide solution at room temperature. [e] Calculated for D_{2d} or T_d cube via the force field given in Table V. [f] Numbers in parentheses are observed or calculated downshifts upon ^{34}S substitution for the bridging atoms.

$Bu)_4]^{2-}$ in two different salts,[9b] with $Me_3NCH_2Ph^+$ and Et_4N^+ counterions. The core is appreciably compressed in the former (*l* = 2.315 Å, *s* = 2.252 Å are the mean values for the long and short Fe–S^b bonds) but much less compressed in the latter (*l* = 2.294 Å, *s* = 2.274 Å). The present result suggests that if there is any distortion from T_d symmetry for the benzyl cube in solution it is much less than that in the Et_4N^+ salt (*l* = 2.310 Å, *s* = 2.239 Å).

Even if there is no J–T effect in the ground state, there might well be one in some of the excited states. The manifestation of a dynamical J–T effect in RR spectra is intensification of the J–T-active mode,[46] which maintains its polarization. It is possible that the 268-cm^{-1} RR band of benzyl cube in solution is the (weakly) J–T-activated E mode. The band appears to be depolarized, although its weakness makes the polarization measurement quite uncertain. Another candidate for this band is the T_1 mode, which can be activated via vibronic coupling ($T_2 \times T_2 = A_1 + E + T_1 + T_2$). It should display inverse polarization, contrary to the experimental evidence. However, the issue is further complicated by the likely coincidence of an internal ligand mode, seen in the IR spectrum at 268 cm^{-1} (Figure 2). This mode is no doubt polarized, and to the extent that is contributes to the 268-cm^{-1} RR band it reduces the apparent depolarization ratio. Thus a T_1 assignment cannot be ruled out.

The 268-cm^{-1} frequency is coincident with the 270-cm^{-1} band of the crystalline sample, assigned to the $A_2(T_1)$ component, and substantially displaced from the 298-cm^{-1} crystal band assigned to the $A_1(E)$ component. Thus an appreciable energy shift is implied if the E mode is at 268 cm^{-1} in solution. This shift, however, is seen in the normal mode coordinate calculations. In the T_d calculation the E and T_1 modes are *both* close to 268 cm^{-1}, and it is on this basis that we tentatively assign both modes to the 268-cm^{-1} solution band. Although their calculated frequencies can be raised somewhat by adjusting the force constants, it is difficult to separate the two frequencies to any appreciable extent. Separation is provided naturally in the D_{2d} calculations, however, the compression along the $\bar{4}$ axis serving to drive the E mode energy up. Thus the calculations emphasize the sensitivity of the E mode, both in frequency and intensity, to the D_{2d} distortion.

Excitation Profiles. The electronic spectra of 4-Fe proteins are characterized by broad bands at 290 and 380–400 nm.[1] According to the calculation of Aizman and Case,[7c] the first of these should be assigned to a group of $S^b \rightarrow$ Fe charge-transer transitions, while the second involves transitions from filled orbitals with mainly Fe–S^t character to empty orbitals with mainly Fe–S^b character. The mixed character of these latter transitions may account for the lack of any pronounced discrimination in the enhancement of Fe–S^t vs. Fe–S^b RR bands with excitation in the visible region.

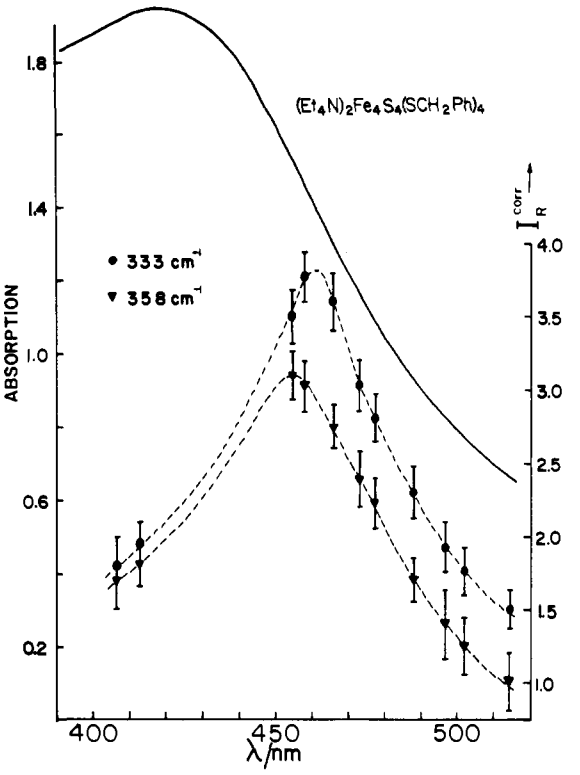

Figure 7. Excitation profiles for 333- and 358-cm^{-1} Raman bands of $(Et_4N)_2[Fe_4S_4(SCH_2Ph)_4]$ superimposed on the electronic spectrum. Raman band intensities were determined relative to the dimethylacetamide 430-cm^{-1} band.

Figure 7 compares excitation profiles (EPs) for the $[Fe_4S_4(SCH_2Ph)_4]^{2-}$ 333-cm^{-1} A_1 Fe–S^b and the 358-cm^{-1} T_2 Fe–S^t bands with the absorption spectrum in the 400–500-nm region.

(46) Siebrand, W.; Zgierski, M. Z. In *Excited States*; Lim, E. C., Ed.; Academic: New York, 1979; Vol. 4, pp 1–136.

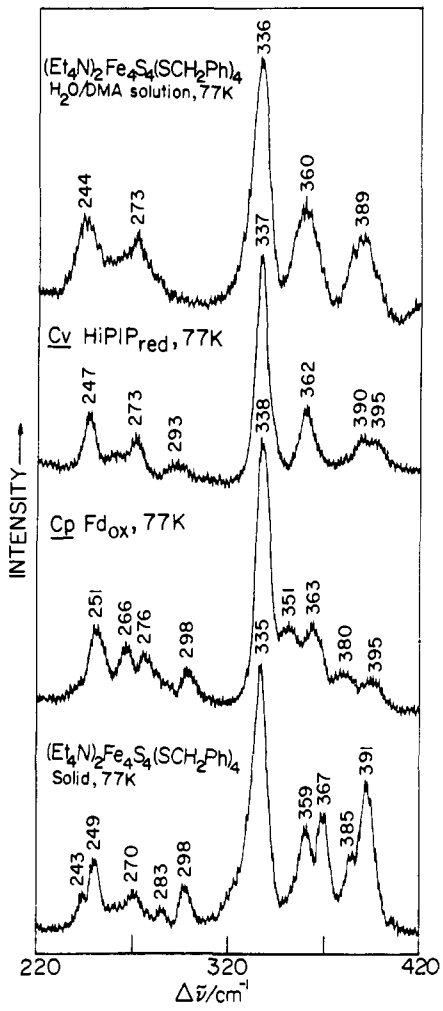

Figure 8. Low-temperature resonance Raman spectra (77 K) of *Cp* Fd_{ox} (λ_{ex} = 4880 Å), *Cv* $HiPIP_{red}$ (λ_{ex} = 4880 Å), and $(Et_4N)_2[Fe_4S_4(SCH_2Ph)_4]$ in solution (λ_{ex} = 4579 Å) and solid state (λ_{ex} = 4880 Å). The protein samples (~2 mM) were in 0.05 M Tris–HCl buffer, pH 7.5. The analogue complex samples were in a KCl pellet or in an aqueous detergent medium, consisting of 90/5/5 (vol %) H_2O/DMA/Triton X-100. All spectra were obtained via backscattering from a liquid-N_2 dewar. For these data the spectrometer was advanced in 0.5-cm^{-1} increments, slit widths 5 cm^{-1}.

The RR intensities were obtained by using the 430-cm^{-1} band of *N,N*-dimethylacetamide as an internal standard. The two RR bands track each other fairly closely, although the EP maximum for the 333-cm^{-1} band is slightly (~5 nm) blue-shifted relative to the 358-cm^{-1} band. It is curious that the profiles are as similar as they are since the scattering mechanisms must be different: A-term scattering for the A_1 mode, and B-term scattering for the T_2 mode.

The most striking aspect of the EPs, however, is their failure to track the absorption spectrum. Although the absorption rises to a broad maximum at 420 nm, the RR intensity peaks at ~450 nm and drops sharply at shorter wavelengths. The likeliest explanation for this fall-off is that contributions to the RR tensor from the lower and higher energy transitions within the absorption band interfere with one another due to opposing phases of the transition moments, leading to intensity cancellation. From a practical perspective it is clear that the absorption maximum is not the best wavelength for examining RR spectra of $[Fe_4S_4X_4]^{2-}$ species.

4-Fe Proteins: Fd and HiPIP. *Cp* ferrodoxin (Fd) and *Cv* high potential iron proteins (HiPIP) are paradigmatic for the two classes of Fe_4S_4-containing proteins, with low (−350 to −450 mV) and high (ca. +350 mV) redox potentials. Their crystal structures have been determined and their properties have been examined in some detail. In the generally accepted three-state model of

Table V. Force Constants (mdyn/Å) for a $Fe_4S_4{}^bS_4{}^t$ Cube in D_{2d} and T_d Symmetry[a]

D_{2d} symmetry[b]		T_d symmetry[c]	
$K(Fe\text{–}S^b)_8(l)$	0.950	$K(Fe\text{–}S^b)_{12}$	0.950
$K(Fe\text{–}S^b)_4(s)$	1.130		
$K(Fe\text{–}S^t)_4(t)$	1.400	$K(Fe\text{–}S^t)_4$	1.40
$H(\Delta\alpha)_{12}$	0.0	$H(\Delta\alpha)_{12}$	0.0
$H(\Delta\beta)_{12}$	0.170	$H(\Delta\beta)_{12}$	0.170
$H(\Delta\gamma)_{12}$	0.250	$H(\Delta\gamma)_{12}$	0.250
$F(S^b\cdots S^b)_8$	0.050	$F(S^b\cdots S^b)_{12}$	0.05
$F(S^b\cdots S^b)_4$	0.042		
$F(S^b\cdots S^t)_4$	0.050	$F(S^b\cdots S^t)_{12}$	0.05
$F(S^b\cdots S^t)_8$	0.042		
$F(Fe\cdots Fe)_4$	0.095	$F(Fe\cdots Fe)_{12}$	0.110
$F(Fe\cdots Fe)_8$	0.115		

[a] K stretching; H bending, F repulsive gem nonbonded interaction. S^b and S^t are bridging and terminal sulfurs, respectively. The subscripts 4, 8, and 12 refer to the number of internal coordinates which share this force constant. [b] The crystallographic benzyl cube structure parameters, listed in the caption for Figure 1, were used. [c] For this calculation all Fe–S^b were set at ~2.31 Å and Fe–S^t at 2.251 Å; all other parameters were adjusted slightly to maintain T_d symmetry.

Table VI. Resonance Raman Frequency (cm^{-1}) and ^{34}S Shift Comparison for Ferredoxin and HiPTP with Solid and Solution $(Et_4N)_2[Fe_4S_4(SCH_2Ph)_4]$

D_{2d} assignment	solid[a] cube	Fd[b]	HiPIP[c]	solution[d] cube	T_d assignment
		Mainly Terminal ν(Fe–S)			
A_1	391 (1)[e]	395 (3.9)	397	384 (1)	A_1
$B_2(T_2)$	367 (1)	351 (0.7)	362	358 (1)	T_2
$E(T_2)$	359 (2)	363 (2.0)			
		Mainly Bridging ν(Fe–S)			
$B_2(T_2)$	385 (6)	380 (5.6)	390	384 (1)	T_2
$E(T_2)$					
A_1	335 (8)	338 (7.0)	337	333 (7)	A_1
$A_1(E)$	298 (5)	298 (4.9)	293	268 (3)	E
$B_1(E)$	283 (4)	276 (4.5)	273		
$E(T_1)$	283 (4)	276 (4.5)	273	268 (3)	T_1
$A_2(T_1)$	270 (3)	266 (4.0)			
$E(T_2)$	243 (5				
$B_2(T_2)$	249 (6)	251 (6.2)	249	241 (6)	T_2
$E(T_2)$	243 (5)				

[a] $(Et_4N)_2[Fe_4S_4(SCH_2Ph)_4]$ in KCl pellet at low temperature (77 K). [b] Oxidized *Cp* ferredoxin in frozen solution (77 K). [c] Reduced *Cv* HiPIP in frozen solution (77 K). [d] $(Et_4N)_2[Fe_4S_4(SCH_2Ph)_4]$ in *N,N*-dimethylacetamide solution at room temperature. [e] Numbers in parentheses give downshifts upon ^{34}S substitution for the bridging S atoms.

Fe_4S_4 proteins,[47] oxidized Fd and reduced HiPIP, both of which have diamagnetic ground states, are at the same oxidation level, $[Fe_4S_4]^{2+}$, as the analogues $[Fe_4S_4](SR)_4]^{2-}$ (average oxidation state $Fe^{2.5+}$ if S^b counts as S^{2-}).

RR spectra of oxidized Fd and reduced HiPIP in frozen solution are compared in Figure 8 with spectra of benzyl cube in the Et_4N^+ salt and in frozen H_2O/DMA solution. The last spectrum is better resolved than that of room temperature DMA solution (Figure 5) and the frequencies are shifted up by 2–5 cm^{-1}, but there are no other alterations. There is a remarkable resemblance between the spectra of *Cp* Fd and the crystalline $(Et_4N)_2[Fe_4S_4(SCH_2Ph)_4]$. There is a one-to-one correspondence for all bands in the two spectra, except that the weak E component of the low-frequency T_2 Fe–S^b mode at 243 cm^{-1} is not detectable in the Fd spectrum. The correspondence extends as well to the $^{34}S^b$ isotope shifts, which could be obtained quite accurately with ^{34}S-reconstituted Fd (Figure 9). All of the shifts were the same within experimental error, as shown in Table VI. There is, however, an interesting reversal of the ^{34}S shifts for 363/351-cm^{-1} bands of the protein relative to the 367/359-cm^{-1} bands of benzyl cube, indicating a reversal of the $B_2/E(T_2)$ assignments (see Table IV). This reversal, and also the differences in the frequencies

(47) Carter, C. W.; Kraut, J.; Freer, S. T.; Alden, R. A.; Sieker, L. C.; Adam, A.; Jensen, L. H. *Proc. Natl. Acad. Sci. U.S.A.* **1972**, *69*, 3526–3529.

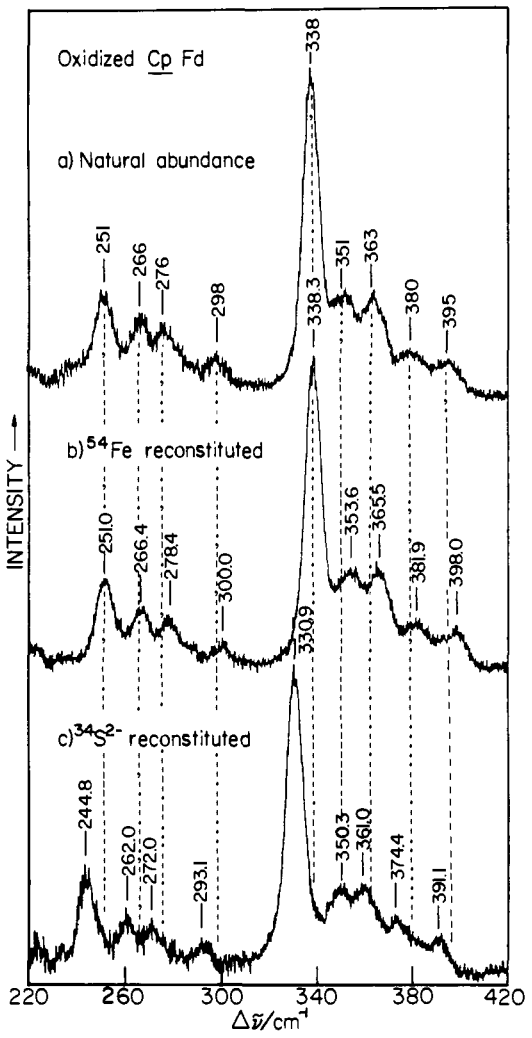

Figure 9. Low-temperature (77 K) resonance Raman spectra of *Cp* Fd_{ox} and its $^{34}S^{2-}$ and ^{54}Fe substituted proteins obtained with 4880 Å Ar^+ laser excitation (250 mW) and 5 cm^{-1} slit widths. For these data the spectrometer was advanced in 0.2-cm^{-1} increments at 1 s per point.

themselves, probably reflects differences in thiolate conformation between protein and analogue. We also took the opportunity to reconstitute *Cp* Fd with ^{54}Fe to obtain the ^{54}Fe isotope shifts (Figure 9) used in the normal mode calculation. As noted above, these shifts do not distinguish terminal and bridging modes, since the Fe atoms are equally involved in both. They do, however, help identify the A_1 (338 cm^{-1}) and low-frequency T_2 (251 cm^{-1}) bridging modes, which have particularly small observed, and calculated, ^{54}Fe shifts. These modes involve relatively small amplitudes of Fe motion (see Figure 5).

The crystal structure of *Pa* Fd does reveal D_{2d} distortions for the two Fe_4S_4 clusters, according to the analysis of Jensen and co-workers.[3] The reported Fe–S bond length differences are comparable (*l*, *s* = 2.27, 2.20 Å for one cluster and 2.26, 2.15 Å for the other) to those seen for $(Et_4N)_2[Fe_4S_4(SCH_2Ph)_4]$[13] (*l*, *s* = 2.310, 2.239 Å). The RR evidence fully supports the existence of this distortion in Fd. On the other hand, the single Fe_4S_4 cluster in HiPIP was also reported to be distorted.[4] Analysis of the crystal structure led Carter[48] to conclude that the Fe–S bond lengths could similarly be divided into a group of eight long ones, 2.36 Å, and four short ones, 2.25 Å, with a standard deviation of the mean of 0.02 Å. The *Cv* HiPIP spectrum, however, is essentially the same as that observed for benzyl cube in solution (Figure 8). Neither spectrum show any splittings for the T_2 Fe–S modes. Some distortion of the *Cv* HiPIP Fe_4S_4 cube may be reflected by activation of the E cluster made which is seen weakly near 293 cm^{-1}. However, the overall spectral pattern is much closer to that expected for a Td cluster.[49] It seems likely that the error level of the HiPIP crystal structure fitting is now low enough to be confident about bond distance differences at the level of 0.1 Å or less, even for the strongly scattering Fe and S atoms.

It is uncertain whether the structural difference between Fd and HiPIP seen in the RR spectra is significant at the level of protein functions. The plasticity of the Fe_4S_4 core suggested by the range of Fe–S distances seen in different $(Fe_4S_4)X_4^{2-}$ crystal structures suggests that not much energy is required to produce the distortion evident in the Fd spectrum. The large HiPIP–Fd difference in redox potential cannot be explained on this basis. It is possible, however, that the observed distortion reflects the influence of protein forces which are themselves energetically important. A plausible role for H bonding in tuning the redox potential has been proposed by Carter et al.[4b] A larger number of H bond interactions involving the sulfur atoms is seen for Fd than for HiPIP,[11b] and this is expected to make the $[Fe_4S_4]^+$ oxidation level of reduced Fd more accessible than that for HiPIP. Perhaps these extra H bonds also play a role in producing the D_{2d} symmetry lowering of the core.

Acknowledgment. We thank Drs. M. Cusanovich, M. W. W. Adams, and T. V. Morgan for donating samples of *Cv* HiPIP and *Cp* Fd and Dr. R. H. Holm for helpful discussions. This work was supported by National Institutes of Health Grant GM 13498.

Registry No. $(Et_4N)_2[Fe_4S_4(SCH_2Ph)_4]$, 52523-51-0; $PhCH_2SH$, 100-53-8; $FeCl_2$, 7758-94-3; S, 7704-34-9; Et_4NI, 68-05-3.

(48) Carter, C. W., Jr. *J. Biol. Chem.* **1977**, *252*, 7802–7811.

(49) **Note Added in Proof**: Drs. T. M. Loehr and J. Sanders-Loehr have informed us that RR spectra of HiPIPs other than that from *Cv* show stronger symmetry lowerings (Sanders-Loehr, J.; Loehr, T. M., Mino, Y.; Cusanovich, M., unpublished results).